

Unsupervised ANN-Based Equalizer and Its Trainable FPGA Implementation

Jonas Ney[‡], Vincent Lauinger^{*}, Laurent Schmalen^{*}, and Norbert Wehn[‡]

[‡]*Microelectronic Systems Design (EMS), RPTU Kaiserslautern-Landau, Germany*

{ney, wehn}@eit.uni-kl.de

^{*}*Communications Engineering Lab (CEL), Karlsruhe Institute of Technology (KIT), Germany*

{vincent.lauinger, laurent.schmalen}@kit.edu

Abstract—In recent years, communication engineers put strong emphasis on artificial neural network (ANN)-based algorithms with the aim of increasing the flexibility and autonomy of the system and its components. In this context, unsupervised training is of special interest as it enables adaptation without the overhead of transmitting pilot symbols. In this work, we present a novel ANN-based, unsupervised equalizer and its trainable field programmable gate array (FPGA) implementation. We demonstrate that our custom loss function allows the ANN to adapt for varying channel conditions, approaching the performance of a supervised baseline. Furthermore, as a first step towards a practical communication system, we design an efficient FPGA implementation of our proposed algorithm, which achieves a throughput in the order of Gbit/s, outperforming a high-performance GPU by a large margin.

Index Terms—ANN, Unsupervised, Equalizer, FPGA

I. INTRODUCTION

The goal of next-generation communication systems is not only to increase throughput, lower latency, and improve reliability, but also to enhance autonomy by exploiting artificial neural network (ANN)-based communication algorithms [1], which allow for adaptation to varying channel conditions. Although such algorithms often enhance the communication performance of traditional approaches [2]–[4], the adaptation to changing conditions is based on a huge amount of data, required to perform supervised training of the ANN. This training data needs to be transmitted as pilot symbols, lowering the net throughput and information rate of the communication system. To solve this problem, an ANN-based channel equalizer is proposed in [5], which utilizes a generative adversarial network (GAN) to enable unsupervised training. For unsupervised training, no labels are required, therefore it can be performed without the overhead of transmitting pilot symbols. However, the GAN approach comes with increased computational complexity and instability introduced by an additional ANN serving as loss function.

In this work, a similar approach is presented, but instead of using a discriminator ANN, the training of the ANN-based equalizer is performed using a novel low-complexity unsupervised loss function. After initial supervised training, it

allows for adaptation to varying channel conditions, with the advantages of operating in a blind and channel-agnostic way. However, for a practical baseband processing system, not only the communication performance but also the implementation complexity needs to be analyzed. Therefore, we present a custom hardware architecture of the unsupervised ANN-based equalizer. As hardware platform, we select field programmable gate arrays (FPGAs) as they offer arbitrary precision datatypes, custom datapaths, as well as huge bit-level parallelism. Furthermore, FPGAs are highly flexible as the hardware can be reconfigured, for instance, to adapt to different application requirements. Additionally, an FPGA design is a first step towards a custom application-specific integrated circuit (ASIC) as used in practical communication systems.

In contrast to most previous works [6]–[8], we do not only propose an optimized implementation of the ANN’s forward pass (FP) but also tackle the challenges of implementing the backpropagation algorithm on the FPGA, which enables online retraining on the edge device itself, to adapt for varying channel conditions. A related approach is also presented in [9], but contrary to our work their model is based on the split-step solution of the Manakov-PMD equation instead of an ANN, thus it is not channel-agnostic. Further, it is trained in a supervised way.

In summary, we propose a novel unsupervised loss function and demonstrate its performance for changing channel conditions. Additionally, we present the corresponding FPGA architecture and show that it can achieve Gbit/s throughput, outperforming high-end graphics processing unit (GPU) implementations.

II. SYSTEM MODEL

A digital communication system consists of a transmitter and a receiver with the goal of reliably transmitting information over a noisy channel. The transmitted vector \mathbf{x} , consisting of symbols $x_i \in \mathcal{A}$ from an alphabet $\mathcal{A} = \{A_1, \dots, A_M\}$, is distorted by a channel and results in a received vector \mathbf{y} . At the receiver, an equalizer is applied to \mathbf{y} which aims to revert the distortion introduced by the channel to allow for decisions $\hat{\mathbf{x}}$ which reliably reproduce the transmitted vector \mathbf{x} . Conventionally, the equalizer is either implemented based on a linear finite impulse response (FIR) filter or as decision-

This work was carried out in the framework of the CELTIC-NEXT project AI-NET-ANTILLAS (C2019/3-3) and was funded by the German Federal Ministry of Education and Research (BMBF) under grant agreements 16KIS1316 and 16KIS1317 as well as under grant 16KISK004 (Open6GHuB).

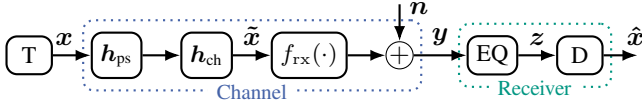


Fig. 1. Model of the communication chain: Data symbols x are sent from a transmitter T over a channel to a receiver R .

feedback equalizer (DFE). In our case, it is represented by a convolutional neural network (CNN).

A. Channel Model

As shown in Fig 1, in our channel model, the transmitted symbols x are convolved with a raised-cosine (RC) pulse shaping filter h_{ps} and a linear channel impulse response h_{ch} to produce \tilde{x} . Specific receiver characteristics can be described by a possibly nonlinear function $f_{rx}(\cdot)$. The received vector y is superimposed by a Gaussian noise vector n . Finally, a decision D is taken based on the equalizer's output z . Since oversampling is essential to real systems, we run all simulations at an oversampling rate of $N_{os} = 2$ samples per symbol (sps).

We consider a dispersive optical channel with intensity modulation with direct detection (IM/DD) and pulse-amplitude modulation (PAM) as described in [10]. The square-law detection (SLD) at the receiver distorts the signal nonlinearly and is modeled by $\tilde{y} = f_{rx}(\tilde{x})$ with $\tilde{y}_i = |\tilde{x}_i|^2$. Linear channel distortions are caused by chromatic dispersion (CD), which can be described by its frequency response

$$H_{cd}(L_{\text{fiber}}, f) = \exp\left(-\frac{1}{2}\alpha L_{\text{fiber}} + j2\pi^2\beta_2 f^2 L_{\text{fiber}}\right),$$

where L_{fiber} is the fiber length, $\beta_2 = -\frac{\lambda^2}{2\pi c} D_{cd}$ is defined by the wavelength λ , the speed of light c and the fiber's dispersion coefficient D_{cd} ; α is the fiber attenuation. This work considers C-band transmission at $\lambda = 1550$ nm over a standard single-mode fiber (SSMF), with $D_{cd} = 17$ ps \cdot nm $^{-1}$ \cdot km $^{-1}$, $\alpha \triangleq 0.2$ dB \cdot km $^{-1}$, and $L_{\text{fiber}} = 30$ km. Thermal noise can be modeled as additive white Gaussian noise (AWGN) with zero-mean and the variance σ_n^2 . For the simulation, we fix the signal-to-noise ratio (SNR) to 20 dB. At the receiver, we carry out hard decision based on the minimum Euclidean distance.

B. ANN Topology

Our ANN topology is completely based on one-dimensional convolution (1D-Conv) layers, which resemble the structure of conventional digital filters. Non-linearity is introduced by rectified linear unit (ReLU) functions following each convolutional layer but the last. In each layer, padding is added to match the size of the output feature map to that of the input. As the data is upsampled by a factor of two before transmission, the last 1D-Conv layer is performed with a stride of two. Thus, one output of the CNN corresponds to the prediction of one transmitted symbol. Our investigations have shown that a model with three 1D-Conv layers and a kernel size of 21 is sufficient. A larger model did not lead to significant gains in communication performance.

III. LOSS FUNCTION

For training the ANN, we use a two-step approach. First, initial training for a channel model is performed in a PyTorch environment based on supervised mean-squared-error (MSE) loss. In a second step, we perform retraining of the ANN on the edge device itself, to adapt to varying channel conditions. This retraining can either be performed with supervised MSE loss or using a custom unsupervised loss function.

The main purpose of the novel, unsupervised heuristic loss function is to enable adaptation of the CNN without any pilot symbols, resulting in less overhead and a higher net data rate. Since the unsupervised loss function does not consider the mapping of the output to the correct symbol, but only operates on the statics of the channel output, the supervised loss function is used for initial training.

A. Novel Unsupervised Loss Function

As a first step, we show how our unsupervised loss function can be applied to PAM-2 modulation. Subsequently, we propose a way to adapt it to PAM-4 modulation.

1) *PAM-2 modulation*: The unsupervised loss function is comprised of two parts, $\text{loss}_a(z)$ and $\text{loss}_b(z)$. First, a polynomial function $p(\cdot)$ is used to push each of the CNN's outputs to the actual constellation points A_1 and A_2 :

$$p(z_n) = (z_n - A_1)^2 \cdot (z_n - A_2)^2.$$

Then $\text{loss}_a(z)$ is given as the sum of $p(z_n)$ over all outputs z_n for a sequence of length N :

$$\text{loss}_a(z) = \sum_{n=1}^N p(z_n).$$

As shown in Fig. 2, $p(z_n)$ has global minima at A_1 and A_2 which correspond to the possible input symbols of the transmitted vector x . Thus, the outputs of the CNN are pushed to one of the undistorted symbols. Since the CNN is initially trained in a supervised fashion, the channel output z_i is mapped to the actual transmitted symbol x_i at the beginning of the unsupervised training. We expected that $\text{loss}_a(z)$ forces the network to keep z_i at the corresponding transmitted symbol x_i even if the channel changes during unsupervised training.

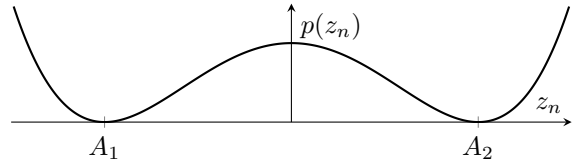


Fig. 2. Polynomial function, with minima at constellation points A_1 and A_2 .

However, we observed that during training all received symbols z were either pushed to the minimum A_1 or to the minimum A_2 . Thus we propose a second loss function $\text{loss}_b(z)$ which forces z to be equally spread between A_1 and A_2 . Therefore, we define d_i as the accumulated absolute distance of

each output of one sequence with length N to the constellation point A_i :

$$d_i = \sum_{n=1}^N |z_n - A_i|.$$

Subsequently, we determine the absolute difference of the distances to A_1 and A_2 , as

$$\text{loss}_b(\mathbf{z}) = |d_1 - d_2|.$$

Thus $\text{loss}_b(\mathbf{z})$ is minimal for $d_1 = d_2$, which is the case when all outputs z_n are equally distributed between A_1 and A_2 . Finally, $\text{loss}(\mathbf{z})$ is calculated as

$$\text{loss}(\mathbf{z}) = \text{loss}_a(\mathbf{z}) + \mu \cdot \text{loss}_b(\mathbf{z}),$$

where μ is a weighting factor to balance between $\text{loss}_a(\mathbf{z})$ and $\text{loss}_b(\mathbf{z})$ (μ is set to 4 in our experiments).

To summarize, our heuristic unsupervised loss function forces the equalizer output to be close to the constellation symbols and equally spread between them. Since the constellation symbols represent the channel input, the equalizer learns to resemble this input at its output. Therefore, by unsupervised training, the outputs are prevented from drifting during changing channel conditions, resulting in an increased communication performance, as shown in Sec. V

2) *PAM-4 modulation*: In addition to the PAM-2 based loss function, we demonstrate how the unsupervised loss function can be adapted to higher-order modulation schemes e.g. PAM-4. The first part of the loss function $\text{loss}_a(\mathbf{z})$ is similar to the PAM-2 example, but with minima at each of the four constellation points A_1, A_2, A_3, A_4 :

$$\text{loss}_a(\mathbf{z}) = \sum_{n=1}^N \prod_{i=1}^4 (z_n - A_i)^2.$$

In contrast, a modification is needed for $\text{loss}_b(\mathbf{z})$. As explained previously, $\text{loss}_b(\mathbf{z})$ is introduced to equally distribute all outputs \mathbf{z} across the constellation points based on the accumulated distance of each output to each constellation point. For PAM-4, $\text{loss}_b(\mathbf{z})$ is constructed based on four distances d_i , one for each constellation point A_i . Further, we define $c(A_i)$ as the distance of A_i to the remaining constellation points:

$$c(A_i) = \sum_{j=1, j \neq i}^4 (|A_i - A_j|)$$

Then $c(A_2) = c(A_3) = 4$ and $c(A_1) = c(A_4) = 6$, as shown in Fig. 3. Thus, for compensation d_2 and d_3 are multiplied by $\frac{3}{2}$:

$$\text{loss}_b(\mathbf{z}) = \left| d_1 - d_4 \right| + \left| \frac{3}{2}d_2 - \frac{3}{2}d_3 \right| + \left| d_1 - \frac{3}{2}d_2 \right| + \left| d_4 - \frac{3}{2}d_3 \right|.$$

This way, $\text{loss}_b(\mathbf{z})$ is minimal if the outputs of the network are equally distributed between A_1 to A_4 . Similar to PAM-2, the final loss is given as the sum of $\text{loss}_a(\mathbf{z})$ and $\text{loss}_b(\mathbf{z})$ with a weighting factor μ .

IV. IMPLEMENTATION

As a first step towards a practical communication system, we present an efficient FPGA implementation of our proposed algorithm.

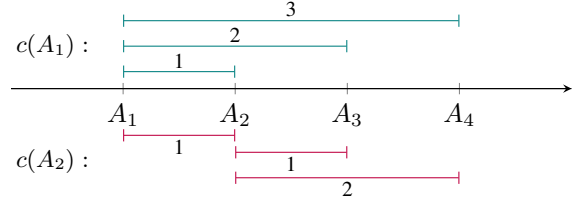


Fig. 3. Illustration of $c(A_1)$ and $c(A_2)$ for PAM-4, with a distance of one between each constellation point.

A. Quantization

For minimizing the implementation complexity, all values of the CNN's FP and backward pass (BP) are represented as quantized fixed-point numbers. To find the optimal bit width for each layer, we perform an in-depth quantization analysis for weights, activations, multipliers, accumulators, and gradients.

In a first step, we select an appropriate quantization scheme for weights and activations by adapting the automatic quantization strategy proposed in [11]. Therefore, the loss function is modified to simultaneously learn the precision of each layer while optimizing the accuracy of the ANN during training. This is achieved by using a differentiable interpolation of the bit-widths, which allows to train them using backpropagation. Similar to [11], we include a trade-off factor in the loss function, which determines how aggressively to quantize. This enables efficient exploration of the trade-off between bit width and communication performance.

Fig. 4 shows the quantization analysis for the PAM-2 channel with a symbol rate of 25 GBd and the model described in II-B. The dotted line connects the Pareto optimal points, where each is trained with a different trade-off factor. For implementation, we selected the model marked by the red square, as it achieves a low BER (0.0006) with moderate complexity (10.1 bits in average). Moreover, a higher number of bits didn't show any improvement in communication performance.

In contrast to the quantization of weights and activations, the quantization of accumulators, multipliers, and gradients can't be learned during training. Therefore, we simulate inference and training for multiple randomly generated input sequences. We

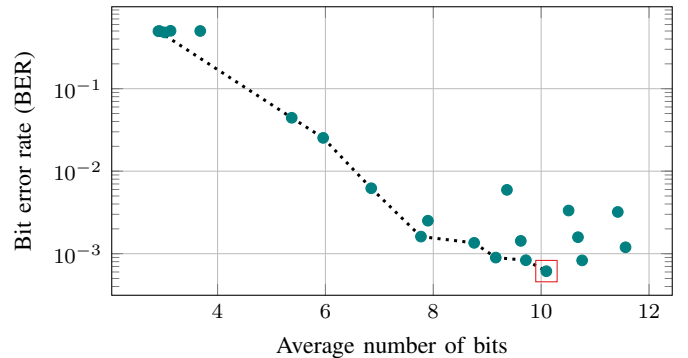


Fig. 4. Plot of the average number of bits used for weights and activations vs BER achieved with this quantization. The dotted line represents the Pareto front, connecting all points with the best trade-off between complexity and accuracy. The red square marks the final model used for implementation.

select the integer and decimal bits for each datatype, as the minimal number of bits needed to cover the whole dynamic range of values profiled in our simulation.

B. Hardware Architecture

A major constraint for high-performance hardware implementation of ANNs is the restricted on-chip memory of the FPGA. The quantization presented in Sec. IV-A is a first step to reduce the memory footprint. However, in contrast to most previous works, we also implement the training of the ANN on the FPGA, which requires additional resources. To perform backpropagation, a large amount of memory is required to store the feature maps of the FP to be reused in the BP. For large sequence lengths, the FPGA’s on-chip memory is usually not sufficient to store those feature maps, thus offloading to external DRAM is necessary, resulting in a limited throughput. In particular, for an implementation with a sequence length of five Ethernet packages, the feature map buffers of one CNN instance nearly consume 50% of the block random access memory (BRAM) resources of the *Xilinx ZCU102*. This limits the memory available for the network’s weights as well as the achievable throughput, as fewer CNN instances can be placed on the board.

To solve this problem, we propose a fully pipelined architecture in which we balance the lifetime of the feature maps such that the memory footprint is reduced, as sketched in Fig. 5.

In our hardware architecture, all modules of the FP (shown in green) and the BP (shown in blue) are implemented as separate pipeline stages. The forward blocks (Conv) calculate the discrete convolution of input i with kernel k and apply the ReLU activation function

$$o = \text{ReLU}(i * k). \quad (1)$$

The backward blocks (CalcGrad) consist of two modules: one to calculate the input’s gradient (CalcInGrad) and another one

to calculate the kernel’s gradient (CalcKGrad). The input’s gradient ∇i is given as the channel-wise convolution of the flipped kernel with the output gradient ∇o :

$$\nabla i = \text{flip}(k) * \nabla o, \quad (2)$$

while the kernel gradient ∇k can be obtained by convolving the input with the output gradient:

$$\nabla k = i * \nabla o. \quad (3)$$

The core of our hardware architecture is a highly customizable convolutional module, which allows for variable kernel size, padding, stride, and dilation. Each convolution of the CNN is implemented as a separate hardware module, enabling parallel computation of each layer and therefore increasing the overall throughput, which is crucial for high-performance communication systems.

To solve the problem of large feature map buffers between the FP and BP, we take advantage of the sequential nature of convolution operations (2) and (3) in the BP. The calculation of ∇i and ∇k can already start before all elements of i and ∇o are available. Since the FP and the BP are implemented as separate pipeline stages, they can be processed in parallel. Therefore, the feature maps are read and written concurrently and the size of the buffers can be greatly reduced. Moreover, we designed our layers in such a way that FP and BP have similar latency. Hence, the size of the feature map buffers is determined only by the depth of the pipeline and does not depend on the length of the sequence. This enables processing symbol sequences of arbitrary length. Thus our approach is suited for many different application scenarios.

To increase flexibility even further, our architecture enables variable degree of parallelism (DOP) on the level of input channels, output channels, kernel size, and the number of instances. This way, the number of multiply-accumulate (MAC) operations performed per clock cycle can be adjusted as required. On the one hand, this enables optimizing the utilization of available hardware resources and thus increases efficiency. On the other hand, variable DOP allows to trade-off power consumption against throughput to adapt to specific application requirements by reconfiguration of the FPGA.

V. RESULTS

The following results are evaluated based on the channel described in Sec. II-A with the ANN topology of Sec. II-B.

A. Adaptation Analysis

As the main purpose of our approach is the adaptation to varying channel conditions on the edge device, we evaluate how supervised and unsupervised retraining of the CNN-based equalizer improves the communication performance. The baseline of our analysis corresponds to a model that is trained from scratch for every new channel condition. Further, we give results for a model which is only trained for the initial channel but not retrained for the changing conditions. We also show the BER for unsupervised and supervised retraining of the

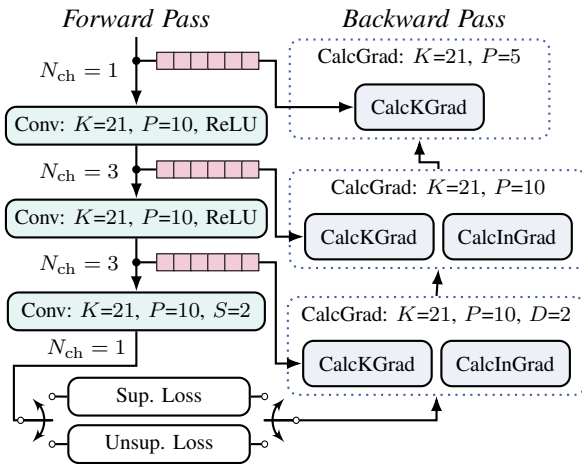


Fig. 5. Hardware architecture with kernel size K , padding P , stride S , dilation D and number of channels N_{ch} . Arrows indicate streams of feature maps, either between subsequent layers or between FP and BP. Feature map buffers are shown in red.

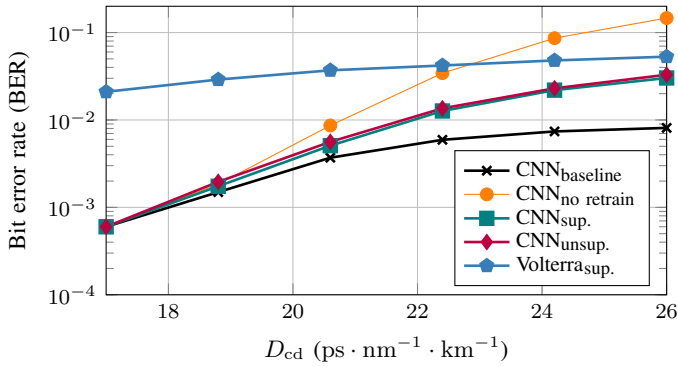


Fig. 6. Results for the PAM-2 channel with a symbol rate of 25 Gbd. Initial training is performed for $D_{cd} = 17 \text{ ps} \cdot \text{nm}^{-1} \cdot \text{km}^{-1}$. $\text{CNN}_{\text{sup.}}$ and $\text{CNN}_{\text{unsup.}}$ are retrained in steps of $1.8 \text{ ps} \cdot \text{nm}^{-1} \cdot \text{km}^{-1}$.

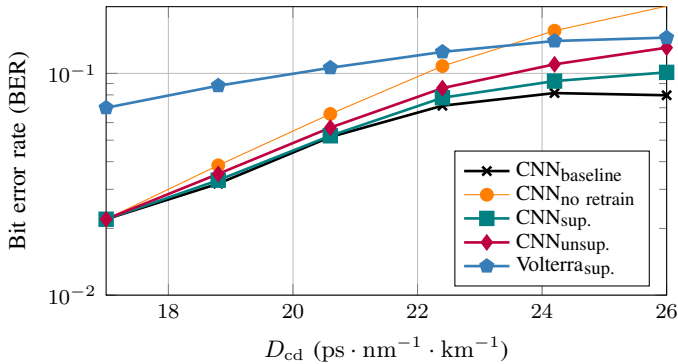


Fig. 7. Results for the PAM-4 channel with a symbol rate of 20 Gbd for different D_{cd} . Initial training is performed for $D_{cd} = 17 \text{ ps} \cdot \text{nm}^{-1} \cdot \text{km}^{-1}$. $\text{CNN}_{\text{sup.}}$ and $\text{CNN}_{\text{unsup.}}$ are retrained in steps of $1.8 \text{ ps} \cdot \text{nm}^{-1} \cdot \text{km}^{-1}$.

CNN, performed during the channel variation. Those models are retrained for 500 iterations with a learning rate of 0.02 with stochastic gradient descent (SGD). We also evaluate the BER of a third-order Volterra equalizer [12] with memory $F = [35, 17, 9]$ and, for fair comparison, approximately the same number of parameters as our CNN, which is trained in a supervised way based on the MSE loss. As a varying channel characteristic, we select the fiber dispersion parameter D_{cd} . This property of the optical fiber may change due to temperature, aging effects, and other environmental factors. The results are shown in Fig. 6 and Fig. 7 for PAM-2 and PAM-4 respectively. As expected, for both cases the BER increases significantly for high D_{cd} if no retraining is performed. Especially the gap to the baseline, which is trained from scratch, grows dramatically. However, by retraining the model in unsupervised fashion, the gap to the baseline can be highly reduced. Specifically, it is decreased by a factor of 6 for $D_{cd} = 26 \text{ ps} \cdot \text{nm}^{-1} \cdot \text{km}^{-1}$ for PAM-2, and by a factor of 2 for PAM-4. For PAM-2 the performance of unsupervised retraining is similar to the supervised one, whereas supervised retraining has a slightly better performance for PAM-4. This indicates that our unsupervised loss function is well suited for performing adaptation to varying channel conditions, especially for PAM-2.

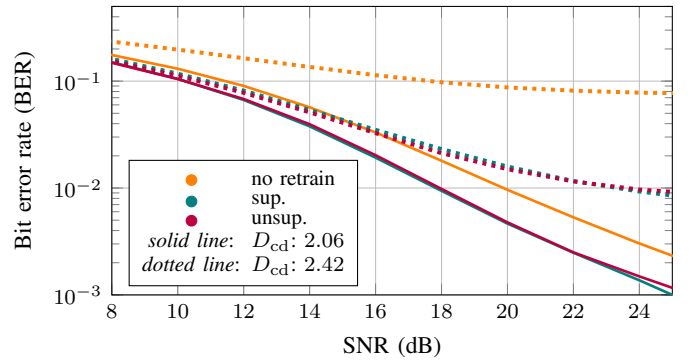


Fig. 8. BER vs SNR for retrained and non-retrained CNNs after D_{cd} changed from $17 \text{ ps} \cdot \text{nm}^{-1} \cdot \text{km}^{-1}$ to 2.06 and $2.42 \text{ ps} \cdot \text{nm}^{-1} \cdot \text{km}^{-1}$ respectively.

In contrast to the supervised loss function, no labeled training data in form of pilot symbols is required, which increases the overall information rate.

Moreover, both retraining techniques outperform the conventional, supervised Volterra equalizer over the whole range of D_{cd} for PAM-2 and PAM-4, validating the potential of ANN-based equalization from a communication perspective.

An additional comparison is shown in Fig. 8, where the performance of the non-retrained CNN is compared with the models retrained for a D_{cd} of $2.06 \text{ ps} \cdot \text{nm}^{-1} \cdot \text{km}^{-1}$ and $2.42 \text{ ps} \cdot \text{nm}^{-1} \cdot \text{km}^{-1}$ for different SNRs. It can be seen that for a D_{cd} of $2.06 \text{ ps} \cdot \text{nm}^{-1} \cdot \text{km}^{-1}$, the retrained models continuously outperform the non-retrained one by around 2 dB. For a D_{cd} of $2.42 \text{ ps} \cdot \text{nm}^{-1} \cdot \text{km}^{-1}$, the gap is even higher, as the non-retrained BER flattens at around 8×10^{-2} . For a BER of 1×10^{-1} , the gain of the retrained CNNs is around 7 dB.

B. Hardware Performance

In the following, we give the implementation results of our hardware architecture described in Sec. IV-B for PAM-2. For FPGA implementation, *Vivado HLS* in combination with *Vivado Design Suite 2019.2* is used and the results are compared to the same CNN running on two GPUs: the high-performance GPU *Nvidia RTX 2080* and the embedded GPU *Nvidia Xavier AGX*. We implement our FPGA architecture on the *ZCU102* evaluation board for a frequency of 300 MHz. The power corresponds to the dynamic power given by Vivado Power Estimation Tool. For the GPU, the dynamic power is obtained using *nvidia-smi*. The batch size of the GPU implementations is increased until the GPUs run out of memory, while the DOP of the FPGA is adjusted to achieve maximal resource utilization. The results are shown in Tab. I, where additionally to power and throughput, the time for retraining for a varying fiber dispersion factor, as discussed in V-B is given.

It is to note that a fair comparison to previous ANN FPGA implementations is not straightforward, as they are either based on a different topology, a different target platform or do not provide an implementation of the ANN training.

As compared to the GPUs, our FPGA architecture outperforms both implementations by orders of magnitude with

TABLE I
HARDWARE IMPLEMENTATION RESULTS

Platform	TP (Mbit)	P (W)	Retraining time (ms)	LUT (%)	DSP (%)	BRAM (%)
ZCU102	1200	4.83	3.3	80.2	69.4	15.8
RTX 2080	140	58	29	-	-	-
AGX Xavier	11.8	3.8	340	-	-	-

respect to throughput and retraining time. Compared to the RTX 2080, the FPGA's throughput is 10 times higher, while the AGX Xavier is outperformed by a factor of 100. The dynamic power consumption of the FPGA architecture is slightly higher than that of the embedded GPU, whereas it increases by a factor of 10 for the high-performance GPU. One reason for the low throughput achieved by the GPUs is the small size of the ANN, which results in a high batch size required to fully utilize the GPU. Thus, the memory bandwidth becomes the bottleneck of the GPU implementations.

In Fig. 9 we demonstrate the flexibility of our FPGA architecture. Each point corresponds to an implementation with a different DOP which can be loaded onto the FPGA. It can be seen that our architecture and FPGA as a platform allow to adapt to different application requirements regarding power consumption and retraining time. Those requirements could for example be imposed by a limited energy budget of the device or by the coherence time of the channel. In particular, the power consumption of [1] is $14\times$ lower than that of [756], while its retraining time is $750\times$ higher. In between there exist multiple Pareto optimal points, which can also be loaded onto the same FPGA. Moreover, power consumption and retraining time could be further reduced as indicated by the red arrows. It is important to highlight, that during retraining, the net datarate is only decreased for the supervised loss. For our novel unsupervised loss function, there is no downtime of the communication, as no labels need to be sent.

In summary, the results demonstrate that our architecture is adjustable to different application requirements like low power

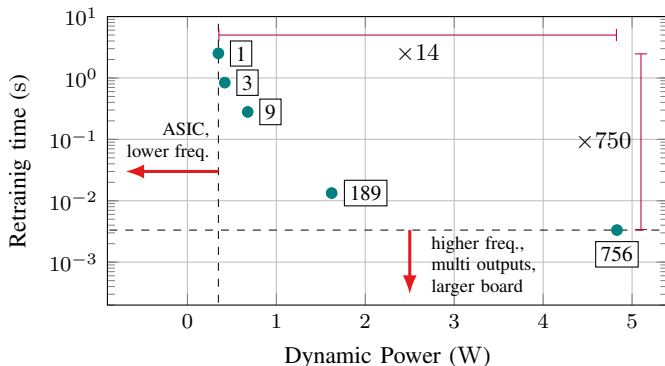


Fig. 9. Dynamic power consumption and time to perform retraining for changing channel conditions on the FPGA for different DOP. The DOP, corresponding to the parallel calculated MAC operations in one layer, is given in the rectangle next to each point.

(order of 100 mW) and high throughput (order of Gbit/s). Our hardware implementation of a trainable ANN-based equalizer is considered a proof-of-concept and a first step towards practical systems in the field of optical communication. In future work, higher throughput could be achieved by designing an ASIC and applying further optimizations, using a higher number of parallel outputs or more instances of the ANN.

VI. CONCLUSION

In this work, we propose a novel approach for unsupervised retraining of an ANN-based equalizer for changing channel conditions. Therefore, we present an unsupervised loss function for PAM-2 and PAM-4 modulation and demonstrate its ability to adapt to a varying fiber dispersion parameter. Furthermore, we present a pipelined FPGA architecture of our approach, to bridge the gap between ANN-based communication algorithms and efficient hardware implementation. As a result, we demonstrated that our unsupervised approach nearly reaches the communication performance of supervised retraining, while reducing the overhead of pilot symbols as labels. Moreover, we show that a throughput in the order of Gbit/s is feasible with our FPGA implementation, which can't be achieved by a high-end GPUs, while it is also highly flexible.

REFERENCES

- [1] C.-X. Wang, M. D. Renzo, S. Stanczak, S. Wang, and E. G. Larsson, "Artificial intelligence enabled wireless networking for 5G and beyond: Recent advances and future challenges," *IEEE Wireless Commun. Mag.*, vol. 27, no. 1, pp. 16–23, 2020.
- [2] A. Zerguine, A. Shafi, and M. Bettayeb, "Multilayer perceptron-based DFE with lattice structure," *IEEE Transactions on Neural Networks*, vol. 12, no. 3, pp. 532–545, 2001.
- [3] M. Schaedler, C. Bluemm, M. Kuschnerov, F. Pittalà, S. Calabrò, and S. Pachnicke, "Deep neural network equalization for optical short reach communication," *Applied Sciences*, vol. 9, no. 21, 2019.
- [4] J. Ney, B. Hammoud, S. Dörner, M. Herrmann, J. Clausius, S. ten Brink, and N. Wehn, "Efficient FPGA implementation of an ANN-based demapper using cross-layer analysis," *Electronics*, vol. 11, no. 7, 2022.
- [5] V. Lauinger, M. Hoffmann, J. Ney, N. Wehn, and L. Schmalen, "Blind and channel-agnostic equalization using adversarial networks," in *Proc. GLOBECOM*, 2022.
- [6] N. Kaneda, C.-Y. Chuang, Z. Zhu, A. Mahadevan, B. Farah, K. Bergman, D. Van Veen, and V. Houtsuma, "Fixed-point analysis and FPGA implementation of deep neural network based equalizers for high-speed PON," *J. Lightw. Technol.*, vol. 40, no. 7, pp. 1972–1980, 2022.
- [7] M. Li, W. Zhang, and Z. He, "FPGA implementation of time-interleaved pruning neural network equalizer for short reach optical interconnects," *Proc. ACP*, 2021.
- [8] P. J. Freire, M. Anderson, B. Spinnler, T. Bex, J. E. Prilepsky, T. A. Eriksson, N. Costa, W. Schairer, M. Blott, A. Napoli, and S. K. Turitsyn, "Towards FPGA implementation of neural network-based nonlinearity mitigation equalizers in coherent optical transmission systems," *Proc. ECOC*, 2022.
- [9] K. Liu, E. Borjeson, C. Hager, and P. Larsson-Edefors, "Fpga implementation of multi-layer machine learning equalizer with on-chip training," *arXiv Preprint*, 2023. [Online]. Available: <https://arxiv.org/pdf/2212.03515.pdf>
- [10] D. Plabst, F. J. García Gómez, T. Wiegart, and N. Hanik, "Wiener filter for short-reach fiber-optic links," *IEEE Commun. Lett.*, vol. 24, no. 11, pp. 2546–2550, 2020.
- [11] M. Nikolic, G. B. Hacene, C. Bannon, A. D. Lascorz, M. Courbariaux, Y. Bengio, V. Gripon, and A. Moshovos, "Bitpruning: Learning bitlengths for aggressive and accurate quantization," *arXiv Preprint*, 2020. [Online]. Available: <https://arxiv.org/abs/2002.03090>
- [12] N. Stojanovic, F. Karinou, Z. Qiang, and C. Prodaniuc, "Volterra and Wiener equalizers for short-reach 100G PAM-4 applications," *J. Lightw. Technol.*, vol. 35, no. 21, pp. 4583–4594, 2017.